



Cite this: *Sens. Diagn.*, 2026, 5, 83

## Adapting antibody-invertase fusion protein immunoassays to multiwell plates for infectious disease antibody quantification

Elysse Ornelas-Gatdula, <sup>a</sup> Xinran An, <sup>bc</sup>  
 Jamie B. Spangler, <sup>bcdefghi</sup> and Netzahualcóyotl Arroyo-Currás <sup>†\*aj</sup>

Traditional enzyme-linked immunosorbent assays (ELISAs) rely on horseradish peroxidase (HRP)-conjugated antibodies to generate a colorimetric response proportional to target antibody concentration. However, spectrophotometric quantification requires expensive benchtop equipment, limiting its usability for frequent, population-scale immunity screening. To overcome this barrier, we previously developed LC15, an antibody-invertase fusion protein that catalyzes sucrose-to-glucose conversion in proportion to antibody levels. This fusion protein enabled antibody quantification using handheld glucometers – affordable, widely available devices already integrated with telehealth infrastructure. Unlike commercial ELISAs, which report relative antibody titers, LC15 facilitates absolute antibody quantification ( $\mu\text{g mL}^{-1}$ ), enhancing applications such as epidemiological monitoring and convalescent plasma dosing. To increase the number of clinical samples processed in a single run of the assay, in this study we transitioned from poly(methyl methacrylate) strips to microwell plates, optimizing pH conditions and reagent concentrations. This adaptation yielded similar sensitivity to the original strip-based assay, but with a 5-fold reduction in reagent consumption and in plasma, as opposed to serum used for the previous study. Using the SARS-CoV-2 receptor binding domain (RBD) as the antigen, we applied LC15 in a 96-well plate format to screen 72 clinical samples in triplicate for anti-RBD antibodies. A blinded comparison with commercial ELISAs demonstrated strong linear correlation ( $R^2 = 0.85$ ) over four orders of magnitude in concentration. By combining accuracy with accessibility, this approach has the potential to facilitate population-level immunity assessments, supporting rapid public health responses in future outbreaks.

Received 1st July 2025,  
 Accepted 8th October 2025

DOI: 10.1039/d5sd00117j

rsc.li/sensors



<sup>a</sup> Chemistry-Biology Interface Program, Zanvyl Krieger School of Arts & Sciences, Johns Hopkins University, Baltimore, MD 21218, USA

<sup>b</sup> Department of Chemical and Biomolecular Engineering, Johns Hopkins University, Baltimore, MD 21205, USA

<sup>c</sup> Translational Tissue Engineering Center, Johns Hopkins University School of Medicine, Baltimore, MD 21205, USA

<sup>d</sup> Department of Biomedical Engineering, Johns Hopkins University School of Medicine, Baltimore, MD 21205, USA

<sup>e</sup> Bloomberg-Kimmel Institute for Cancer Immunotherapy, Johns Hopkins University, Baltimore, MD 21205, USA

<sup>f</sup> Sidney Kimmel Comprehensive Cancer Center, Johns Hopkins University, Baltimore, MD 21205, USA

<sup>g</sup> Department of Oncology, Johns Hopkins University School of Medicine, Baltimore, MD 21205, USA

<sup>h</sup> Department of Ophthalmology, Johns Hopkins University School of Medicine, Baltimore, MD 21205, USA

<sup>i</sup> Department of Molecular Microbiology & Immunology, Johns Hopkins University Bloomberg School of Public Health, Baltimore, MD 21205, USA

<sup>j</sup> Department of Pharmacology and Molecular Sciences, Johns Hopkins University School of Medicine, Baltimore, MD 21205, USA. E-mail: narroyo@unc.edu

<sup>†</sup> Current address: Department of Chemistry, University of North Carolina at Chapel Hill, Chapel Hill, NC 27514, USA.

## Introduction

Enzyme-linked immunosorbent assays (ELISAs) are used to detect antibodies or antigens with high specificity. Chemical conjugation of various enzymes, such as alkaline phosphatase (ALP), glucose oxidase (GOx), and horseradish peroxidase (HRP), using glutaraldehyde as the coupling agent, to human immunoglobulin G (IgG) is a benchmark strategy originally developed to detect intracellular antigens and antibodies for histological purposes.<sup>1</sup> ALP and HRP utilize substrates, *para*-nitrophenyl phosphate (nPP) and 3,3',5,5'-tetramethylbenzidine (TMB), respectively, that change color when interacting with the enzyme and ELISAs exploit this attribute. In 1971, the first ELISA was reported utilizing sheep-anti-rabbit-IgG serum as the immunosorbent immobilized on microcrystalline cellulose and rabbit IgG chemically conjugated to ALP as the detection antibody.<sup>2</sup> In the same year, an ELISA was developed for human chorionic gonadotropin (HCG). Samples containing HCG were coupled to HRP and then incubated with rabbit anti-HCG immobilized on microcrystalline cellulose.<sup>3</sup> Enzymatic activity

for ALP and HRP conjugates were assessed *via* spectrophotometry as their substrates changed color proportional to the amount of enzyme present, allowing for a clinically relevant estimation of the target protein in a sample. While still not as sensitive as radioimmunosorbent assays, ELISAs offer two distinct advantages. First, the enzyme-antibody chemical conjugates can be kept frozen and maintain their enzymatic activity even after months of storage. Second, the workflow and instrumentation required for ELISAs make them more feasible in a clinical setting.<sup>2,3</sup>

Most commercially available secondary detection antibodies are produced *via* a stochastic chemical conjugation with ALP or HRP. As it is not ensured that each antibody present in the reaction will conjugate with the same number of enzyme units, ELISAs utilizing these enzymes can only report relative antibody titers.<sup>4,5</sup> This limitation becomes critical when precise quantification of antibody concentration is medically necessary. For instance, in determining the appropriate dose of convalescent plasma (CCP) for treating acutely ill patients, relative titers do not provide the actual  $\text{mg kg}^{-1}$  antibody dose required for therapeutic efficacy. In a post-clinical trial study, we demonstrated that our glucometer-based ELISA could quantify high-titer anti-S-RBD IgG in CCP donors and recipients in absolute terms.<sup>6</sup> This enabled clinical researchers to compare antibody dosages between CCP and monoclonal antibody treatments, revealing that the effective concentration of anti-S-RBD in CCP was 100- to 1000-fold lower than that of monoclonal antibodies. In addition, the spectrophotometric measurement of color intensity requires costly optics that are not amenable to decentralized, population-scale screening of immunity (see cost analysis in SI document, Tables S1 and S2).

In 2022, we reported an antibody-invertase fusion protein (LC15) in which two invertase proteins are genetically fused to an anti-human immunoglobulin (Ig) G antibody at the C-terminus of the light chains by a flexible  $(\text{G}_4\text{S})_3$  linker.<sup>7</sup> The invertase coupled to LC15 converts molecules of sucrose to glucose when bound to target antibodies in a sample. Due to the genetic fusion of invertase to the anti-human IgG, the problem of stochastic coupling as seen with ALP- and HRP-conjugated secondary antibodies is circumvented, and the stoichiometric control enables glucometer-based antibody quantification, as the concentration of glucose ( $\text{mg dL}^{-1}$ ) is directly proportional to the target antibody load ( $\mu\text{g mL}^{-1}$ ). The electrochemical ELISA utilizing LC15 was originally developed using poly(methyl) methacrylate strips (Fig. 1A), and its efficacy was successfully demonstrated by quantifying anti-severe acute respiratory syndrome coronavirus 2 (SARS-CoV-2) spike protein receptor-binding domain (RBD) antibody (Ab) concentrations among two training sets of clinical samples.<sup>7</sup> However, the assay itself was cumbersome, partly due to the difficulty of immobilizing the receptor-binding domain (RBD) antigen onto plastic strips. Immobilization required an overnight incubation with a hydrogel, which was then followed by an overnight incubation with RBD. In

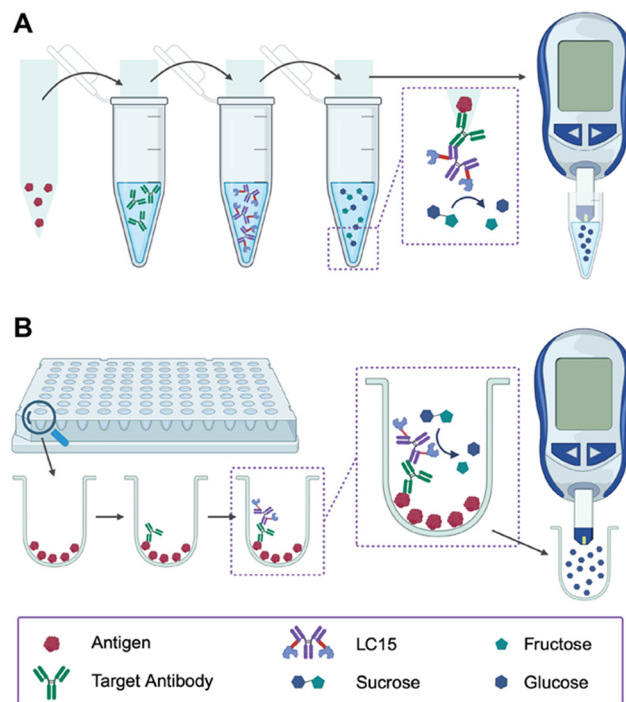


**Fig. 1** Translation of electrochemical ELISA from test-strip based to multiwell plate format. (A) The original assay was developed on poly(methyl) methacrylate strips functionalized with the antigen. The strips were moved from tube to tube containing the reagents for each immunoassay step.<sup>7</sup> (B) In this study we migrated the assay to a polystyrene 96-microwell plate that follows a more traditional workflow of an indirect ELISA, with the antigen passively adsorbed onto the surface of the plate, with reagents added and washed away in a stepwise manner.

addition, the strips needed to be moved from one solution to the next throughout the assay, limiting the number of samples that could be analyzed in a single day.

In this study, we increased the number of clinical samples that could be analyzed during a single run of the assay by migrating our platform from the plastic strips to a multiwell plate format (Fig. 1B). Flat-bottom plates are used in colorimetric ELISAs as they provide an even surface that is necessary for optical measurements in a plate reader. While the difference in signal output between flat and round-bottom plates is modest and most pronounced at higher antigen concentrations (Fig. S1), round-bottom plates offer a slightly larger surface area for antigen immobilization. Since our platform does not rely on optical measurements, we elected to use 96-well round-bottom plates to take advantage of this geometric feature and maximize assay performance within the constraints of our format. We optimized our platform using RBD as our antigen to detect anti-RBD Ab to compare its performance against the original plastic strip-based platform. RBD is a small protein with multiple epitopes for antibody binding; however, most of these epitopes are all relatively close to each other and their accessibility is dependent on orientation or conformation.<sup>8,9</sup> The anti-RBD antibody



CR3022, used in our study, binds a highly conserved epitope on RBD with high affinity ( $K_D = 6.3$  nM).<sup>10</sup> The proximity of the epitopes on RBD to each other and the high binding affinity between RBD and CR3022 makes this a suitable antigen–antibody pair when determining antibody concentrations in clinical samples *via* ELISA, even if there may be other antibodies present in the sample that recognize other epitopes.<sup>11</sup>

The multiwell plate format minimizes antigen deposition periods and allows for long-term storage of antigen-coated plates. Additionally, through various modifications to the original reagents of our assay, we significantly increased sensitivity and signal output, while reducing the amounts of antigen and detection antibody required. We validated the efficacy of this format in a blind study utilizing plasma samples from a clinical study that were also subjected to traditional ELISA screening. The congruency of our data against titer levels indicates that this format is a reliable method for quantifying antibody concentrations in clinical samples.<sup>6</sup> Finally, we also demonstrate that LC15 is able to bind other human IgGs, by quantifying antibodies (anti-spike Ab) against the SARS-CoV-2 full-length spike protein.

## Results and discussion

Translating the glucometer-based immunoassay from the original strip test to a multiwell plate format resulted in higher sensitivity for the detection of antibodies with lower consumption of reagents. To illustrate this and for convenience (*i.e.*, to reduce the need for recombinant LC15 preparation), we first reoptimized all assay parameters using a commercially purchased horseradish peroxidase (HRP)-conjugated reporter and spectrophotometric detection (Fig. 2). The assay steps consisted of coating the plate wells with antigen (Fig. 2A, bottom left), then incubating the antigen in the presence of target antibody (Fig. 2A, bottom center) and, finally, forming the sandwich with the HRP-conjugated reporter (Fig. 2A, bottom right). To develop and validate our assay we used in-house-produced SARS-CoV-2 receptor binding domain (RBD) for the antigen, as well as a commercially purchased monoclonal anti-RBD antibody [CR3022]. When the target-bound HRP-modified reporter is exposed to a solution containing hydrogen peroxide and tetramethylbenzidine (TMB), HRP catalyzes the reduction of hydrogen peroxide *via* oxidation of the chromogen TMB.<sup>12</sup> This reaction changes the well solution

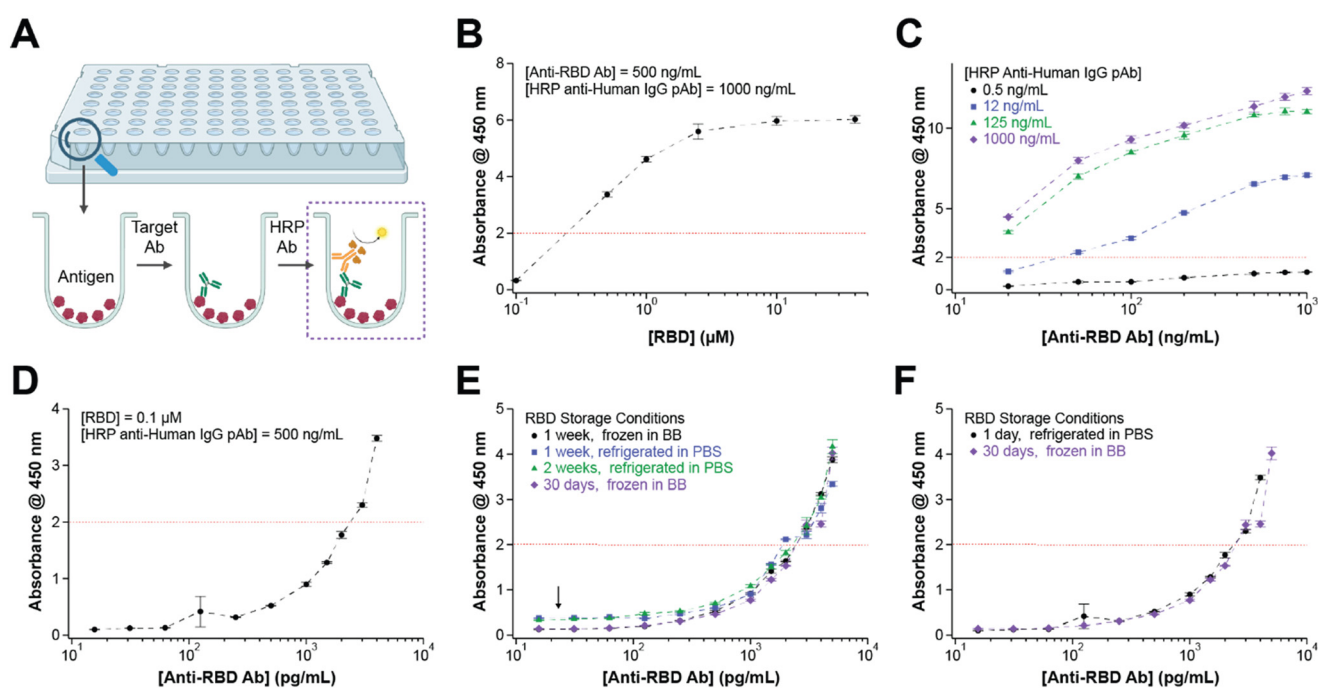


**Fig. 2** Optimization of ELISA parameters using standard HRP-conjugated anti-human IgG. Unless otherwise indicated, incubation times and reagent concentrations were as follows: 18 h for 0.1  $\mu$ M RBD, 1 h for blocking buffer, 30 min for anti-RBD antibody, 30 min for 500 ng  $\text{mL}^{-1}$  HRP anti-human IgG polyclonal antibody, and 10 minutes for TMB. The horizontal dashed red lines indicate an absorbance value of 2, which represents the upper limit of the linear range for absorbance-to-concentration measurements according to Beer's law. Values above this threshold deviate from linearity and are not reliably quantifiable. (A) Workflow for traditional ELISA with an optical output. (B) Antigen loading was more efficient relative to the original strip-based assay (see Fig. S5 from ref. 7), with successful plate coating using (0.1  $\mu$ M vs. 1  $\mu$ M) under saturating concentrations of the target and detection antibodies. (C) Similarly, less detection antibody was needed (500 ng  $\text{mL}^{-1}$  vs. 25  $\mu\text{g mL}^{-1}$ ) to achieve similar signal saturation. (D) Final dose-response curve for anti-RBD antibody spiked into blocking buffer. The limit of detection (LOD), estimated based on 3 $\times$  the standard deviation of the blank, is  $3.8 \pm 0.4$  pg  $\text{mL}^{-1}$  ( $n = 3$ ). (E) When refrigerated, antigen-coated plates generated drift in the assay's LOD over time. When kept frozen, could be successfully used for weeks without LOD drift. (F) Example data demonstrating no significant difference in ELISA output after plate storage, frozen, for 30 days vs. freshly prepared plate.



from colorless to a deep blue in direct proportion to the number of sandwich immunoassays formed in the wells. Here, the colorimetric reaction was quenched after 10 min *via* addition of sulfuric acid, causing the solution to change from the original deep blue color to yellow, prior to quantification at the wavelength of  $\lambda = 450$  nm.

Evaluating the effect of RBD loading to the plate wells, we observed a multifold decrease in protein loading required to achieve the same assay absorbance. Specifically, the original protocol (Fig. 1A) first required poly(methyl methacrylate) strips to be briefly incubated in an antifouling hydrogel followed by an overnight incubation with a coupling carbodiimide agent (EDC) to functionalize the surface for antigen conjugation. This was then followed by a second overnight incubation in an RBD solution at a concentration of 1  $\mu$ M to ultimately generate sufficient oxidized TMB at target saturation to achieve a molecular absorbance of 2 (all volumes and incubation times being equal). In contrast, under identical test conditions, the multiwell polystyrene plate assay achieved comparable molecular absorbance using RBD loaded from an  $\sim$ 250 nM solution, a four-fold reduction relative to the strip-based assay (Fig. 2B). To ensure operation within the linear range of absorbance-to-concentration as described by Beer's law, we selected a 100 nM RBD loading concentration for all subsequent plate-based assays (first data point in Fig. 2B). The reduced antigen requirement in the plate-based assay likely reflects differences in surface interaction mechanisms: the strip-based assay involves chemical conjugation of the antigen to a hydrogel matrix, whereas the plate-based assay relies on passive adsorption onto polystyrene surfaces. Although we did not directly measure the surface area of the hydrogel-coated strips *versus* the plate wells, the hydrogel likely presents a substantially larger microscopic surface area. Nevertheless, the plate-based assay achieved similar glucose production per unit volume with less antigen, suggesting improved antigen utilization efficiency, potentially due to enhanced accessibility or favorable adsorption dynamics.

Migrating the assay from strip format to the multiwell plates also decreased the amount of reporter antibody needed to achieve sensitive immunodetection. To demonstrate this effect, we titrated RBD-modified plates with increasing concentrations of anti-RBD Ab (from 10 to 100 ng  $\text{mL}^{-1}$ ) and finished the sandwich assay with four different concentrations of HRP-modified reporter (0.5, 12, 125 and 1000 ng  $\text{mL}^{-1}$ , Fig. 2C). Our measurements showed that even at the lowest target concentration, a molar absorbance  $>2$  was observed with the two highest reporter concentrations of 125 ng  $\text{mL}^{-1}$  and 1000 ng  $\text{mL}^{-1}$ . For reference, our previous report on the strip assay required an HRP-modified reporter concentration of 25  $\mu\text{g}$   $\text{mL}^{-1}$ , which is between 25 to 200 times higher concentrations, to obtain the same absorbance measurements. Based on these results, we decided to maintain a reporter concentration of 500 ng  $\text{mL}^{-1}$  for all subsequent measurements. Finally, a key outcome of the above-described optimizations is a net improvement in

immunoassay limit of detection (estimated as  $3\times$  the standard deviation of the blank), from  $477.8 \pm 136.5$  pg  $\text{mL}^{-1}$  in the original strip-based assay to  $3.8 \pm 0.4$  pg  $\text{mL}^{-1}$  in the multiwell plate format (Fig. 2D).<sup>7</sup>

To minimize batch-to-batch variability in the immunoassay measurements, we evaluated if preparation of large batches of RBD-modified plates followed by freezing was effective at preserving the plates over time. The idea was that a large batch of plates could be prepared in advance to a study, then the plates could be thawed one by one as needed to complete the full study with a single batch, thereby minimizing error carryover from plate modification. For this purpose, we prepared multiple plates at  $t = 0$ , and evaluated two conditions: (1) storage in phosphate buffered-saline at 4 °C and (2) storage in blocking buffer (5% w/v casein, 0.05% v/v Tween 20, 1× PBS) at  $-20$  °C. We then conducted antibody titrations on such plates after one, two, or four weeks of storage. The resulting spectrophotometric titrations (Fig. 2E) showed comparable target antibody concentrations ( $\sim$ 2 ng  $\text{mL}^{-1}$ ) at a molar absorbance = 2, regardless of storage time. However, the absorbance baseline significantly increased for plates that were stored at 4 °C (black arrow in Fig. 2E). In contrast, plates that were frozen at  $-20$  °C with blocking buffer in the wells produced statistically identical calibrations relative to those obtained on freshly prepared plates at  $t = 0$  (Fig. 2F).

Having established the ideal solution concentration for RBD loading into the wells during antigen deposition (Fig. 2B) and the stability of antigen-modified plates during long term storage in the freezer (Fig. 2F), we proceeded to migrate the assay conditions to our glucometer-based detection using LC15 (Fig. 1, bottom). In this assay, after forming the antibody sandwich we fill the wells with sucrose solution (100 mM). The two invertase molecules present in LC15 then catalyze the conversion of sucrose to glucose and fructose. Finally, glucose is generated in proportion to the number of antibody sandwiches present in the wells and can be quantified using over-the-counter glucometers, obviating the need for expensive photonic detectors.

Integrating LC15 into the new multiwell plate assay from the strip-based assay allowed us to efficiently quantify more antibodies in clinical specimens using a fraction of the antigen (0.1  $\mu$ M *vs.* 1  $\mu$ M) and the LC15 reporter (0.02  $\mu$ M *vs.* 0.1  $\mu$ M, respectively) while maintaining similar limits of detection (9–18 ng  $\text{mL}^{-1}$  *vs.* 10.9 ng  $\text{mL}^{-1}$ ). To demonstrate this, we tested the response of the glucometer to two different concentrations of target antibodies, 200 ng  $\text{mL}^{-1}$  (Fig. 3A, black) and 1000 ng  $\text{mL}^{-1}$  (Fig. 3A, blue), using LC15 solution concentrations between 0.1 and 25  $\mu\text{g}$   $\text{mL}^{-1}$ . For both target antibody concentrations, we observed signal starting to plateau at  $\sim$ 5  $\mu\text{g}$   $\text{mL}^{-1}$ . Relative to the original test strip-based assay, which needed the use of 26.5  $\mu\text{g}$   $\text{mL}^{-1}$  of LC15 to generate 80 mg  $\text{dL}^{-1}$  of glucose at a target antibody concentration of 2.0  $\mu\text{g}$   $\text{mL}^{-1}$ , the same amount of glucose was generated in the wells but only requiring 5.3  $\mu\text{g}$   $\text{mL}^{-1}$  of



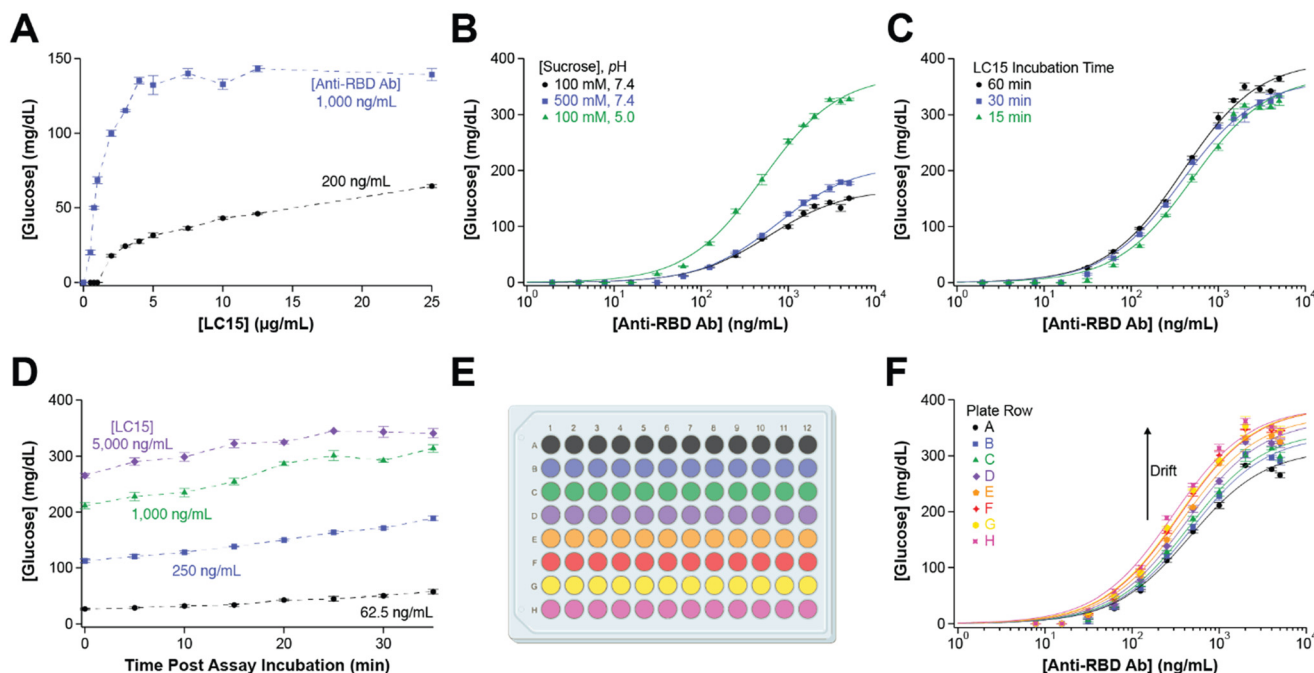


**Fig. 3** Optimization of electrochemical ELISA parameters using LC15 as the detection antibody. Unless otherwise indicated, incubation times and reagent concentrations were as follows: 18 h for 0.1  $\mu$ M RBD, 1 h for blocking buffer, 30 min for anti-RBD antibody, 1 h for 0.02  $\mu$ M LC15, and 1 h for 100 mM sucrose in PBS, pH 5.0. (A) Estimation of [LC15] needed to maximize assay signal output at non-saturating anti-RBD Ab concentrations. Glucose levels were measured after incubation with 100 mM sucrose, pH 7.4. (B) When prepared in PBS, pH 7.4, increasing the concentration of sucrose from 100 mM to 500 mM results in a small increase glucose output. However, invertase enzymatic activity significantly increases when 100 mM sucrose is prepared in PBS, pH 5.0. (C) Longer LC15 incubation periods improve detection sensitivity by  $\sim$ 25%, as determined by comparing EC<sub>50</sub> values across conditions (see Table S4 for statistical analysis). (D) Invertase cannot be quenched and continues to convert sucrose to glucose as the plate is read, resulting in drift over time. (E and F) We addressed drift in the plate readout by building row-based titration curves.

LC15 at a target antibody concentration of 0.46  $\mu$ g mL<sup>-1</sup> (Table S3).

The glucose output of LC15 was doubled by adjusting the solution pH to the optimal value for invertase (pH = 5.0).<sup>13</sup> The previous manuscript reporting LC15 used the reporter at pH = 7.4, a value that is optimal for the glucose oxidase employed in glucose strips, but too alkaline for optimal sucrose to glucose conversion by invertase. Evaluating the effects of decreasing the pH of the sucrose solution to pH = 5.0, we observed a doubling of the amount of glucose produced over the same incubation period (Fig. 3B, green vs. black data). This indicates that the catalytic rate of invertase was significantly increased without appreciably affecting the detection sensitivity of the glucometer. In contrast, increasing the concentration of sucrose by fivefold generated only a modest increase in sucrose conversion (blue vs. black data in Fig. 3B), an indication that invertase is already operating under diffusion control of the substrate. Based on these results, we conducted all subsequent assays using a solution of 100 mM sucrose in phosphate-buffered saline adjusted to pH = 5.0.

The amount of glucose generated in the wells of the plate is a function of target antibody concentration and incubation time. This is illustrated in Fig. 3C, which shows assay calibration curves following 15 min-, 30 min- and 60 min-

long incubations of the completed immunoassays in pH = 5 sucrose solution. At any target antibody concentration point, the glucose output is larger after 60 min-long incubations relative to incubating for 15 min and 30 min. While there is no shift in effective concentration at 50% of the signal output between 30 min and 60 min, a shift is observed between 15 min and 60 min (Table S4). Due to a combination of higher glucose output and effective concentration at 50%, we proceeded with a 60 min-long incubation time for LC15. Unfortunately, the conversion of sucrose by invertase cannot be effectively quenched by an inhibitor and the inhibitors tested also appear to have a negative effect on glucose oxidase (Fig. S2).<sup>14</sup> This results in continuous glucose production at all target antibody concentrations, with higher target concentrations generating more drift (Fig. 3D).

To account for drift in our antibody measurements, we calibrated our multiwell plate assay following a serial full-row approach. To do this, we prepared calibration plates for every condition considered (for example, different sample dilution factors), in which each row corresponded to a full, 12-point calibration curve (Fig. 3E). The data generated in this way (Fig. 3F) reflects the drift caused by the time it takes to serially measure glucose values across an entire plate (the EC<sub>50</sub> values corresponding to all calibrations are included in

Table S5). Given that the plate interrogation time is the same for all assays, we can then use the calibration curve corresponding to each plate row to accurately determine the antibody concentrations of any samples contained within that row in a test plate.

We analytically validated our assay by quantifying the anti-SARS-CoV-2 antibody concentrations of 72 samples from a convalescent plasma study conducted at the Johns Hopkins Hospital. The goal of the study was to determine the empirical dilution factor in circulating antibody concentrations after dosing plasma from convalescent COVID-19 patients to just infected, acutely ill individuals. The results of this study have already been published elsewhere;<sup>6</sup> here, we reanalyzed the samples to demonstrate the high extent of agreement between our multiwell plate, glucometer-based assay and commercial ELISAs. A strong advantage of our assay is that it allows the quantitative determination of actual antibody concentrations, as opposed to the titer levels typically reported by commercial ELISAs. The clinical samples were 100% plasma. We took the samples without further processing and diluted them down to 1% or 20% with blocking buffer, to ensure sufficient dilution was achieved to cover the broad range of antibody concentrations present in the samples. To calibrate our assay, we used blank plasma from confirmed SARS-CoV-2 negative, unexposed, unvaccinated individuals. We built calibration curves by spiking the plasma with increasing concentrations of commercially purchased monoclonal anti-RBD antibody, at the two experimental dilution factors of 1% (Fig. 4A) and 20% (Fig. 4B). Furthermore, we also quantified the antibody levels in donors against the full-length spike protein by building calibration curves for a 20% dilution factor (Fig. S3) in a similar manner as described above by using in-house produced SARS-CoV-2 full-length spike protein and a 1:1:1 mixture of commercially produced RBD (Abcam PN: ab273073), S1 (Novus Biologicals PN: NBP3-07956), and NTD (ACROBiosystems PN: SPD-S164) monoclonal

antibodies. EC<sub>50</sub> values corresponding to all calibrations are included in Tables S6, S7, and S8, respectively, of the SI document.

The clinical samples were initially interrogated for antibody titer by the Sullivan Lab at Johns Hopkins School of Medicine, using a previously published protocol.<sup>15</sup> The samples were then deidentified, randomized, and shipped to our laboratory for cross interrogation *via* our multiwell plate assay. After all measurements were completed, we submitted the results of our antibody quantifications back to the Sullivan Lab for cross validation relative to their titer determinations. The scatter plot resulting from this blinded study (Fig. 4C) demonstrates the high agreement rate between our glucometer-based method and commercial ELISAs, with an overall linear correlation coefficient of 85% at a confidence value  $p \ll 0.01$ . We note that in this scatter plot we converted the target antibody units to  $\text{ng mL}^{-1}$  to coincide in magnitude with the relative scale of area under the curve (AUC) derived from the commercial ELISA measurement performed by the Sullivan Lab. The scaling is arbitrary and does not affect the magnitude of the correlation, as all measure values were scaled equally. In addition, we were able to quantify antibodies against the full-length spike protein and every donor consistently showed a higher concentration of antibodies against full-length spike *versus* RBD alone (Table S9).

## Conclusions

Translating the glucometer-based ELISA to a multiwell plate format enables more efficient screening of clinical samples while also reducing prep time and reagent use when compared to its strip-based counterpart. Due to its versatility, we expect LC15 can be used in place of other reporter anti-human IgGs, particularly in cases when a handheld glucometer is more accessible economically than a plate reader. In addition, the reliability of the glucometer should

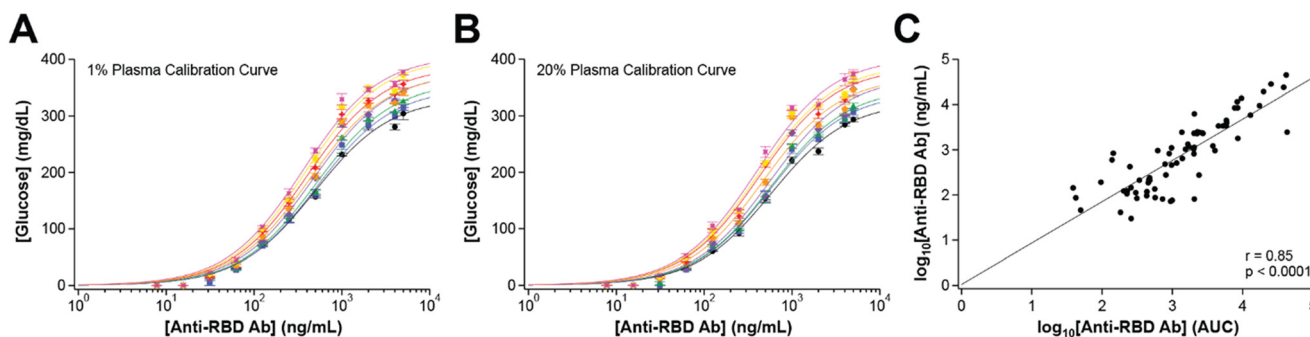


**Fig. 4** Multiwell plate-based electrochemical ELISA successfully measures anti-RBD antibodies in cohort of samples from a convalescent plasma study. Patient plasma was diluted in blocking buffer to either (A) 1% or (B) 20% for the target to stay within detectable range of the assay. Separate dose-response curves were built for these two dilutions, using monoclonal anti-RBD antibody, to account for differences. (C) The AUC for the samples used in this study were determined independently by the Sullivan Lab at the Johns Hopkins School of Public Health. A linear regression against the antibody concentration calculated *via* our electrochemical ELISA shows a positive correlation with an  $R^2 = 0.85$  between the two data sets.



also allow quantitative ELISAs to be performed in environments that may not support the instrumentation required for optical measurements. While smartphone-based imaging approaches have been explored as low-cost alternatives for quantifying colorimetric ELISAs, these methods often require device-specific calibration, controlled lighting conditions, and image processing software, which can introduce variability and limit standardization across different settings. In contrast, consumer-grade glucometers are mass-produced, FDA-approved, and widely integrated into clinical workflows and electronic health record systems. Their consistent performance, ease of use, and regulatory acceptance make them particularly well-suited for decentralized and resource-limited settings. By leveraging this existing infrastructure, our glucometer-based ELISA platform offers a practical and scalable alternative to both benchtop optical readers and experimental smartphone-based systems, with the added benefit of compatibility with established clinical practices.

While we were able to increase efficiency by migrating the original assay from plastic strips to a 96 microwell plate, each well still must be read manually *via* a handheld glucometer, a process that requires approximately 40 minutes for a full plate. This is compounded by our inability to quench invertase at the end of incubation prior to measuring sucrose to glucose conversion with the glucometer. As a result, there is drift in the measurements that must be compensated by generating calibration curves to account for the increase in glucose over time. Despite these limitations, our efforts to address these constraints have yielded highly reproducible calibration curves due to 1) the inherent structure of LC15 that yields a consistent invertase to anti-human IgG ratio and 2) the consistent incubation times for each step of the protocol developed, particularly for the sucrose reporter solution, allowing for a single set of calibration curves to be generated given a set of conditions prior to analyzing clinical samples. These advantages address the lot-to-lot variability that often affects reporter enzymes (e.g. HRP or ALP) chemically coupled to antibodies for ELISAs, causing them to require a full calibration curve to be generated each time the assay is performed.

We have demonstrated the robustness of our platform with respect to an optical-based ELISA *via* the quantification of anti-RBD antibodies. We have also shown that LC15 is capable of binding other human IgGs against different epitopes of the SARS-CoV-2 full-length spike protein. Our team is now directing efforts to demonstrate the utility of LC15 in applications requiring antibody quantification against viral antigens beyond SARS-CoV-2 and for inflammatory cytokines. In parallel, we are developing a higher-throughput electrochemical ELISA platform by automating liquid handling and implementing a method to measure glucose concentrations across multiple wells in a single pass, thereby addressing the limitations and drift associated with the current manual data collection workflow.

## Materials and methods

### Chemicals and reagents

Deionized water used to prepare reagents was first filtered through a Milli-Q water purification system purchased from Millipore Sigma (Darmstadt, Germany). All reagents were brought to room temperature prior to use. 10× PBS, pH 7.4 (BP399-20) and Tween 20 (BP337-500) were purchased from Fisher Bioreagents (Fairlawn, NJ). Casein sodium salt (J6559036) was purchased from Thermo Scientific Chemicals (Ward Hill, MA). A 1× PBS solution was prepared by diluting 10× PBS with water and is used at pH = 7.4 unless otherwise indicated. Wash buffer (WB) is a solution of 0.05% v/v Tween 20 in 1× PBS. Blocking buffer (BB) was prepared by dissolving 5% w/v casein sodium salt in WB and stored at 4 °C until use. 3,3',5,5'-tetramethylbenzidine (TMB) liquid substrate system for ELISA (T0440-100ML), ammonium sulfate (A4915-500G), and sodium sulfate (239313-500G) were purchased from Sigma-Aldrich (Saint Louis, MO). Trace metal grade sulfuric acid (A510-500), trace metal grade hydrochloric acid (T00308-0500), ACS grade ammonium chloride (A661-500), and ACS grade sucrose (S5-500) were purchased from Fisher Chemical (Fair Lawn, NJ). The stop solution used in HRP-based assays was 0.5 M sulfuric acid prepared by diluting the stock with water. Hydrochloric acid was used to adjust 1× PBS to pH = 5.0, monitored *via* an OrionStar A214 pH meter from Thermo Scientific (Beverly, MA) and stored at 4 °C until use. Solutions of 100 mM sucrose were prepared using a 100 mL volumetric flask by dissolving 3.24 g sucrose in 1× PBS, pH 7.4 or 1× PBS, pH 5.0, aliquoted into 15 mL conical centrifuge tubes, and stored at -20 °C until use. A 500 mM sucrose solution was prepared in a 100 mL volumetric flask by dissolving 17.11 g sucrose in 1× PBS, pH 7.4, aliquoted into 15 mL conical centrifuge tubes, and stored at -20 °C until use. Nunc™ 96-well polystyrene round bottom microwell plates (262162) and Nunc™ 96-well polystyrene flat bottom microwell plates (269787) were purchased from Thermo Fisher Scientific (Roskilde, Denmark). 96-well flat bottom plates (655101) were purchased from Greiner Bio-One (Monroe, NC). Sealing tape for 96-well plates (15036) was purchased from Thermo Fisher Scientific (Rockford, IL). The SARS-CoV-2 receptor binding domain (RBD) antigen and LC15 invertase-antibody fusion protein were expressed and purified by the Spangler Lab at Johns Hopkins University according to their previously published protocols.<sup>7</sup> Rabbit anti-human IgG H&L (HRP) (ab6759) and anti-SARS-CoV-2 spike glycoprotein S1 antibody [CR3022] (ab273073) (referred to as HRP anti-human IgG pAb and anti-RBD Ab, respectively) were purchased from Abcam (Waltham, MA).

### Ethical use of clinical specimens

The deidentified human plasma samples were from a previous study and used with permission in accordance with the associated IRB. Johns Hopkins served as the single-IRB (sIRB). For the Center for American Indian Health sites, the protocol was also independently reviewed and approved by



the Navajo Nation Health Human Research Review Board and the National Indian Health Service IRB. The protocol was also approved by the Department of Defense (DoD) Human Research Protection Office (HRPO). An independent medical monitor who was unaware of the trial group assignments reviewed all serious adverse events, and an independent panel of three physicians who were unaware of the trial-group assignments adjudicated Covid 19 related hospitalizations and severity. An independent data and safety monitoring board provided interim safety and efficacy reviews. The trial was conducted in accordance with the principles of the Declaration of Helsinki, the Good Clinical Practice guidelines of the International Council for Harmonisation, and all applicable regulatory requirements. Written and signed informed consent was obtained from all participants.<sup>6</sup>

### Protein expression and purification

The recombinant antibody-invertase fusion protein (LC15) was prepared as described previously,<sup>7</sup> comprising the human immunoglobulin (IgG)-specific mouse IgG2a kappa antibody HP6017, a flexible (G<sub>4</sub>S)<sub>3</sub> linker and a full, intracellular isoform of *Saccharomyces cerevisiae* invertase (UniProt ID, P00724-2) fused to the C-terminus of the antibody light chain (LC) and cloned in gWiz vector (Genlantis). LC15 was expressed recombinantly in human embryonic kidney (HEK) Expi293 cells (Thermo Fisher Scientific) *via* transient co-transfection of plasmids encoding the heavy chain (HC) and LC-invertase fusion proteins of LC15 in a 1:4 ratio. HEK Expi293 cells were grown to a density of  $1.5\text{--}2 \times 10^6$  cells per mL on the day of transfection. Total plasmid DNA and polyethylenimine (PEI MAX® 40 kDa, Kyfora Bio) transfection reagent were mixed in Opti-MEM™ media (Thermo Fisher Scientific) with a concentration of 1  $\mu\text{g mL}^{-1}$  and 5.4  $\mu\text{L mL}^{-1}$  respectively, and incubated at room temperature for 10 min. Subsequently, the DNA/PEI MAX® mixture (100 mL per liter of cells) was added to a flask containing HEK Expi293 cells, which was then incubated at 37 °C with shaking for 5 days. Secreted protein was harvested from HEK Expi293 cell supernatants by Protein G affinity chromatography, followed by size-exclusion chromatography on an ÄKTA™ fast protein liquid chromatography (FPLC) instrument using a Superdex 200 column (Cytiva). The receptor binding domain (RBD) of the wild type severe acute respiratory syndrome coronavirus 2 (SARS-CoV-2) spike protein from the earliest lineage A virus (WT, YP\_009724390.1, residues 319–541; NC\_045512.2, A lineage) was also prepared as described previously.<sup>7</sup> The DNA sequence encoding the RBD protein with a C-terminal hexahistidine (His) tag was cloned into the pCAGGS plasmid.<sup>15</sup> Transient transfection of HEK Expi293 cells proceeded as for LC15. Protein was purified from cell supernatants *via* Ni-NTA (Expedeon) affinity chromatography followed by size-exclusion chromatography on an FPLC instrument using a Superdex 200 column (Cytiva). All

proteins were stored in HEPES-buffered saline (HBS, 150 mM NaCl; 10 mM HEPES; pH 7.3). Purity was verified by SDS-PAGE analysis.

### Antigen adsorption onto multiwell plates and storage

For both HRP and LC15 assays, 0.1  $\mu\text{M}$  (2.5 ng  $\text{mL}^{-1}$ ) RBD was prepared in 1× PBS, pH 7.4 and 50  $\mu\text{L}$  was added to each well of a 96-well plate. The plate was sealed and left to incubate overnight for 18 h at 4 °C. The plate was then brought to RT, flicked over a sink, and patted face down to remove any non-adsorbed RBD. The plate was washed with 150  $\mu\text{L}$  WB, shaken manually for 5 s, flicked over a sink, and patted with a paper towel; this wash cycle was repeated twice more. To block the plate for immediate use, 200  $\mu\text{L}$  of BB was added to each well and allowed to incubate on the ThermoMixer at 25 °C, 500 rpm for 60 min. To block the plate for future use, 200  $\mu\text{L}$  of BB was added to each well, sealed, and stored at -20 °C. Upon use, frozen plates were placed directly from the freezer onto a ThermoMixer at 25 °C, 500 rpm for 70 min. After blocking buffer incubation, both immediate and future use plates were flicked over a sink, patted faced down on a paper towel, and washed with 200  $\mu\text{L}$  WB, shaken manually for 5 s, flicked over a sink, and patted face down on a paper towel; this wash cycle was repeated once more. A final wash is performed with 200  $\mu\text{L}$  WB, shaken on a ThermoMixer at 25 °C, 500 rpm for 1 min, flicked over a sink, and patted with a paper towel. The volumes for BB and WB after blocking for flat bottom plates were increased to 300  $\mu\text{L}$  to minimize non-specific binding due to the larger microwell capacity in this format.

For LC15-based assay for to quantify antibodies against the full-length spike protein, the protocol developed for anti-RBD detection above was also followed. However, to normalize the signal to match that of the anti-RBD Ab only assay, 5 ng  $\text{mL}^{-1}$  full-length spike protein prepared 1× PBS was used to coat the plates.

### IgG detection with HRP for optimization assays

Following RBD adsorption and blocking, anti-RBD Ab commercially purchased from Abcam was prepared to the concentrations listed in Table S10 in BB and 50  $\mu\text{L}$  of each concentration was pipetted into wells in triplicate or quadruplicate. The plate was placed on a ThermoMixer at 25 °C, 500 rpm for 30 min. After incubation, the plate was flicked over a sink, patted face down on a paper towel, and washed with 150  $\mu\text{L}$  WB, shaken manually for 5 s, flicked over a sink, and patted face down on a paper towel; this wash cycle was repeated once more. A final wash is performed with 150  $\mu\text{L}$  WB, shaken on a ThermoMixer at 25 °C, 500 rpm for 1 min, flicked over a sink, and patted with a paper towel.

The HRP Anti-human IgG pAb commercially purchased from Abcam was diluted to 500 ng  $\text{mL}^{-1}$  in BB and 50  $\mu\text{L}$  was added to each well. The plate was placed on a ThermoMixer at 25 °C, 500 rpm for 30 min. After incubation, the plate was flicked over a sink, patted face down on a paper towel, and



washed with 150  $\mu$ L WB, shaken manually for 5 s, flicked over a sink, and patted face down on a paper towel; this wash cycle was repeated once more. A third wash is performed with 150  $\mu$ L WB, shaken on a ThermoMixer at 25 °C, 500 rpm for 5 min, flicked over a sink, and patted with a paper towel. To condition the plate for the substrate, a final wash is performed with 150  $\mu$ L 1× PBS, shaken on a ThermoMixer at 25 °C, 500 rpm for 5 min, flicked over a sink, and patted with a paper towel.

To each well, 50  $\mu$ L of TMB substrate was added and placed on a ThermoMixer at 25 °C, 500 rpm for 10 min. The reaction is then quenched with 150  $\mu$ L 0.5 M H<sub>2</sub>SO<sub>4</sub> and placed on a ThermoMixer at 25 °C, 500 rpm for 1 min. The absorbance is measured at 450 nm using an Implen NanoPhotometer (Westlake Village, CA).

### IgG detection with LC15 for optimization assays

Following RBD adsorption and blocking, anti-RBD Ab commercially purchased from Abcam was prepared to the concentrations listed in Table S11 in BB and 50  $\mu$ L of each concentration was pipetted into wells in triplicate. The plate was placed on a ThermoMixer at 25 °C, 500 rpm for 30 min. After incubation, the plate was flicked over a sink, patted face down on a paper towel, and washed with 150  $\mu$ L WB, shaken manually for 5 s, flicked over a sink, and patted face down on a paper towel; this wash cycle was repeated once more. A final wash is performed with 150  $\mu$ L WB, shaken on a ThermoMixer at 25 °C, 500 rpm for 1 min, flicked over a sink, and patted with a paper towel.

The LC15 antibody-invertase fusion protein provided by the Spangler Lab at Johns Hopkins School of Medicine was diluted to 0.02  $\mu$ M with BB and 50  $\mu$ L was added to each well. The plate was placed on a ThermoMixer at 25 °C, 500 rpm for 30 min. After incubation, the plate was flicked over a sink, patted face down on a paper towel, and washed with 150  $\mu$ L WB, shaken manually for 5 s, flicked over a sink, and patted face down on a paper towel; this wash cycle was repeated once more. A third wash is performed with 150  $\mu$ L WB, shaken on a ThermoMixer at 25 °C, 500 rpm for 5 min, flicked over a sink, and patted with a paper towel. To condition the plate for the substrate, a final wash is performed with 150  $\mu$ L 1× PBS, shaken on a ThermoMixer at 25 °C, 500 rpm for 5 min, flicked over a sink, and patted with a paper towel.

To each well, 50  $\mu$ L of sucrose solution were added and the plate was placed on a ThermoMixer at 25 °C, 500 rpm for 60 min. After incubation, 30  $\mu$ L from each well was transferred to corresponding wells in a flat bottom plate to accommodate the width of the test strip in the measurement step while also minimizing evaporation. A hospital-grade handheld glucometer and glucose test strips donated by Nova Biomedical (Waltham, MA) were used to measure glucose in each well consecutively along each row, starting with row A, column 1.

### Pre-screening clinical samples for anti-RBD Ab to determine dilution

The ELISA protocol used closely follows the LC15 optimization assay. For each clinical specimen, the plasma was diluted to 1%, 10%, and 20% in BB to a final volume of 50  $\mu$ L and each dilution was run singularly. The data was then analyzed to determine the optimal dilution for each clinical specimen by selecting the dilution that fell within 25–250 mg dL<sup>-1</sup> glucose. The clinical samples required either 1% or 20% dilution.

### Generation of LC15 drift-free calibration curves for IgG quantification

The ELISA protocol used closely follows the LC15 optimization assay, but requires three plates and differs in the preparation of the anti-RBD Ab. A set of calibration curves was built for each % plasma dilution (0%, 1%, or 20% confirmed SARS-CoV-2 negative human plasma in BB) by spiking in anti-RBD Ab at the concentrations listed in Table S11. Each of the anti-RBD Ab concentrations was assigned to one of three plates (four concentrations per plate). Each concentration was randomly assigned to three columns so that measurements were done in triplicate for each row. The data from each row among the three plates were pooled to generate a full calibration curve corresponding to that row, as seen in Fig. 3F, 4A and B.

For the anti-spike Ab calibration curves, a 1:1:1 mixture of commercially produced RBD (Abcam PN: ab273073), S1 (Novus Biologicals PN: NBP3-07956), and NTD (ACROBiosystems PN: SPD-S164) monoclonal antibodies was made and then spiked into 20% confirmed SARS-CoV-2 negative human plasma in BB at the concentrations listed in Table S12. Each of the anti-spike Ab concentrations was assigned to one of three plates (four concentrations per plate). Each concentration was randomly assigned to three columns so that measurements were done in triplicate for each row. The data from each row among the three plates were pooled to generate a full calibration curve corresponding to that row, as seen in Fig. S3.

### Anti-RBD Ab quantification of clinical samples

The ELISA protocol used closely follows the LC15 optimization assay. The clinical samples were diluted according to their pre-screen results (1% or 20% in BB) and run in triplicate. All replicates for each clinical specimen were placed in the same row and then averaged to calculate anti-RBD Ab concentration. For example, if the clinical specimen was diluted to 20% and placed in row C, then the corresponding equation derived from the 20% calibration curve for row C (Table S7) would be used to calculate the undiluted concentration of anti-RBD Ab.



## Anti-spike Ab quantification of clinical samples

The ELISA protocol used closely follows the LC15 optimization assay. The donor clinical samples were diluted according to % in BB and ran in triplicate. All replicates for each clinical specimen were placed in the same row and then averaged to calculate anti-spike Ab concentration (Fig. S4). For example, if the clinical specimen was placed in row C, then the corresponding equation derived calibration curve for row C (Table S8) would be used to calculate the undiluted concentration of anti-spike Ab.

## Data processing

Excel was used to calculate the mean and standard error for each set of replicates. The data were then imported into Igor Pro 8.04 from WaveMetrics (Lake Oswego, OR) for plotting and analysis. For Fig. 3B, C, F, 4A and B and S3, the calibration curves were generated using the curve fitting function and applying the Hill equation with base = 0 and rate = 1. For Fig. 4C, the Pearson correlation coefficient was calculated by applying the linear correlation test within the correlation tests function.

## Conflicts of interest

J. B. S. and N. A.-C. have filed patents related to the fusion protein described in this study and its application in electrochemical ELISAs. E. O.-G. and X. A. declare no competing interests.

## Data availability

The data supporting this article have been included as part of the supplementary information (SI). Additionally, all data/files used for the creation of figures is available at the Johns Hopkins Research Data Repository, under a DOI to be published concurrently with this submission.

Supplementary information: the SI document contains additional experimental data, technology cost analyses, and extended tables containing the results from regression analyses and binding measurements, under DOI: <https://doi.org/10.7281/T1NWYUTO>.

## Acknowledgements

This research was supported by funds provided by the Johns Hopkins School of Medicine, the Johns Hopkins University Office of the Provost, Emerson Collective, and the National Science Foundation (Award Number 2143160). E. O.-G. is supported by the NIH grant T32GM080189.

## References

1. S. Avrameas, Coupling of enzymes to proteins with glutaraldehyde. Use of the conjugates for the detection of antigens and antibodies, *Immunochemistry*, 1969, **6**(1), 43–52, DOI: [10.1016/0019-2791\(69\)90177-3](https://doi.org/10.1016/0019-2791(69)90177-3), from NLM Medline.
2. E. Engvall and P. Perlmann, Enzyme-linked immunosorbent assay (ELISA). Quantitative assay of immunoglobulin G, *Immunochemistry*, 1971, **8**(9), 871–874, DOI: [10.1016/0019-2791\(71\)90454-x](https://doi.org/10.1016/0019-2791(71)90454-x), from NLM Medline.
3. B. K. Van Weemen and A. H. Schuurs, Immunoassay using antigen-enzyme conjugates, *FEBS Lett.*, 1971, **15**(3), 232–236, DOI: [10.1016/0014-5793\(71\)80319-8](https://doi.org/10.1016/0014-5793(71)80319-8), (acccessed 2024/12/28), from NLM PubMed-not-MEDLINE.
4. A. Jeanson, J. M. Cloes, M. Bouchet and B. Rentier, Comparison of conjugation procedures for the preparation of monoclonal antibody-enzyme conjugates, *J. Immunol. Methods*, 1988, **111**(2), 261–270, DOI: [10.1016/0022-1759\(88\)90135-4](https://doi.org/10.1016/0022-1759(88)90135-4), from NLM Medline.
5. Y. Luo, M. Pehrsson, L. Langholm, M. Karsdal, A.-C. Bay-Jensen and S. Sun, Lot-to-Lot Variance in Immunoassays—Causes, Consequences, and Solutions, in *Diagnostics*, 2023, vol. 13.
6. H. S. Park, A. Yin, C. Barranta, J. S. Lee, C. A. Caputo, J. Sachithanandham, M. Li, S. Yoon, I. Sitaras and A. Jedlicka, *et al.*, Outpatient COVID-19 convalescent plasma recipient antibody thresholds correlated to reduced hospitalizations within a randomized trial, *JCI Insight*, 2024, **9**(8), e178460, DOI: [10.1172/jci.insight.178460](https://doi.org/10.1172/jci.insight.178460), from NLM Medline.
7. E. K. Leonard, M. Aller Pellitero, B. Juelg, J. B. Spangler and N. Arroyo-Curras, Antibody-Invertase Fusion Protein Enables Quantitative Detection of SARS-CoV-2 Antibodies Using Widely Available Glucometers, *J. Am. Chem. Soc.*, 2022, **144**(25), 11226–11237, DOI: [10.1021/jacs.2c02537](https://doi.org/10.1021/jacs.2c02537), from NLM Medline.
8. W. Tai, L. He, X. Zhang, J. Pu, D. Voronin, S. Jiang, Y. Zhou and L. Du, Characterization of the receptor-binding domain (RBD) of 2019 novel coronavirus: implication for development of RBD protein as a viral attachment inhibitor and vaccine, *Cell. Mol. Immunol.*, 2020, **17**(6), 613–620, DOI: [10.1038/s41423-020-0400-4](https://doi.org/10.1038/s41423-020-0400-4), from NLM Medline.
9. A. Deshpande, B. D. Harris, L. Martinez-Sobrido, J. J. Kobie and M. R. Walter, Epitope Classification and RBD Binding Properties of Neutralizing Antibodies Against SARS-CoV-2 Variants of Concern, *Front. Immunol.*, 2021, **12**, 691715, DOI: [10.3389/fimmu.2021.691715](https://doi.org/10.3389/fimmu.2021.691715), from NLM Medline.
10. X. Tian, C. Li, A. Huang, S. Xia, S. Lu, Z. Shi, L. Lu, S. Jiang, Z. Yang and Y. Wu, *et al.*, Potent binding of 2019 novel coronavirus spike protein by a SARS coronavirus-specific human monoclonal antibody, *Emerging Microbes Infect.*, 2020, **9**(1), 382–385, DOI: [10.1080/22221751.2020.1729069](https://doi.org/10.1080/22221751.2020.1729069), from NLM Medline.
11. W. R. Griswold, Theoretical analysis of the sensitivity of the solid phase antibody assay (ELISA), *Mol. Immunol.*, 1987, **24**(12), 1291–1294, DOI: [10.1016/0161-5890\(87\)90123-4](https://doi.org/10.1016/0161-5890(87)90123-4), from NLM Medline.
12. E. S. Bos, A. A. van der Doelen, N. van Rooy and A. H. Schuurs, 3,3',5,5' - Tetramethylbenzidine as an Ames test negative chromogen for horse-radish peroxidase in enzyme-immunoassay, *J. Immunoassay*, 1981, **2**(3–4), 187–204, DOI: [10.1080/1532181808056977](https://doi.org/10.1080/1532181808056977), from NLM Medline.
13. B. G. Wilkes and E. T. Palmer, Similarity of the Kinetics of Invertase Action in Vivo and in Vitro. II, *J. Gen. Physiol.*,



1932, **16**(2), 233–242, DOI: [10.1085/jgp.16.2.233](https://doi.org/10.1085/jgp.16.2.233), (acccesed 1/21/2025), from NLM PubMed-not-MEDLINE.

14 A. Baseer and S. Shall, Properties of the internal invertase of yeast, *Saccharomyces cerevisiae*, *Biochim. Biophys. Acta*, 1971, **250**(1), 192–202, DOI: [10.1016/0005-2744\(71\)90133-1](https://doi.org/10.1016/0005-2744(71)90133-1), from NLM Medline.

15 F. Amanat, D. Stadlbauer, S. Strohmeier, T. H. O. Nguyen, V. Chromikova, M. McMahon, K. Jiang, G. A. Arunkumar, D. Jurczyszak and J. Polanco, *et al.*, A serological assay to detect SARS-CoV-2 seroconversion in humans, *Nat. Med.*, 2020, **26**(7), 1033–1036, DOI: [10.1038/s41591-020-0913-5](https://doi.org/10.1038/s41591-020-0913-5), from NLM Medline.

